

# Incorporating Rigid Structures in Non-rigid Registration using Triangular B-splines

Kexiang Wang, Ying He, and Hong Qin

Department of Computer Science  
State University of New York at Stony Brook  
Stony Brook, NY 11790-4400, USA  
{kwang|yhe|qin}@cs.sunysb.edu

**Abstract.** For non-rigid registration, the objects in medical images are usually treated as a single deformable body with homogeneous stiffness distribution. However, this assumption is invalid for certain parts of the human body, where bony structures move rigidly, while the others may deform. In this paper, we introduce a novel registration technique that models local rigidity of pre-identified rigid structures as well as global non-rigidity in the transformation field using triangular  $B$ -splines. In contrast to the conventional registration method based on tensor-product  $B$ -splines, our approach recovers local rigid transformation with fewer degrees of freedom (DOFs), and accurately simulates sharp features ( $C^0$  continuity) along the interface between deformable regions and rigid structures, because of the unique advantages offered by triangular  $B$ -splines, such as flexible triangular domain, local control and space-varying smoothness modeling. The accurate matching of the source image with the target one is accomplished through the use of a variational framework, in which a composite energy, measuring the image dissimilarity and enforcing local rigidity and global smoothness, is minimized subject to pre-defined point-based constraints. The algorithm is tested on both synthetic and real 2D images for its applicability. The experimental results show that, by accurately modeling sharp features using triangular  $B$ -splines, the deformable regions in the vicinity of rigid structures are less constrained by the global smoothness regularization and therefore contribute extra flexibility to the optimization process. Consequently, the registration quality is improved considerably.

## 1 Introduction

For the last decade, image registration has become an important technique for various computer vision and medical applications, fusing the information from images acquired either at different times or on multiple modalities. A number of reviews have been documented in [1][2][3]. The earliest attempts made by [4][5] typically restrict the deformation between the corresponding images to be rigid and consider global geometric differences only. Later, non-rigid registration was introduced in [6][7] to additionally cope with local differences, resulting from different anatomy, intraoperative deformation, or distortion induced during imaging process. It is often assumed by the non-rigid registration that the objects in the matching images behave as if they were a single elastic body, *i.e.*, the stiffness is constant everywhere. However, this is rarely the case

when the imaged anatomy contains both rigid and soft structures. A practical clinical example was described in [8] where the shape of the brain changed after subdural electrodes were implanted in a surgical procedure. Neither a single rigid body motion nor a nonlinear model with invariant smoothness can accurately represent the transformation between preoperative and postoperative scans since the electrodes translate and rotate only, while the others deform nonlinearly. Therefore, more appropriate methods are required to combine the modeling of both rigidity and non-rigidity in the recovered transformation. Especially, the  $C^0$  continuity on the borders of rigid structures needs to be simulated correctly for precise registration.

In principle, we could build patient-specific physical model to predict the interaction between rigid structures and soft tissues. However, it is impractical to achieve solution with desired accuracy due to high computational cost and insufficient details on mass, elasticity, and other mechanical properties. The efforts made so far were either based on interpolatory spline scheme or through a variational framework. Little *et al.*[9] incorporated independent rigid objects in a modified thin-plate spline (TPS) based nonrigid registration. Anisotropic landmarks were introduced by Rohr *et al.*[10] to TPS to enforce local rigidity constraints. Duay *et al.*[11] simulated the rigid motions by adaptively adjusting TPS radial basis functions according to local stiffness. Tanner *et al.*[12] represented the deformation using  $B$ -splines and locally couple control points in order to model local rigidities. Most recently, Loeckx *et al.*[13] introduce a penalty term to keep voxel-based rigidities in their variational framework by enforcing the orthogonality of Jacobian matrix. Nevertheless, none of the above approaches, except that in [9], can precisely describe  $C^0$  continuity in the displacement field. In spite of the attempt made in [14], it's not straightforward for thin-plate splines to be incorporated with variational framework, which is quite a powerful tool for intensity-based image registration. On the other hand, tensor-product  $B$ -splines has been widely used for optimization-based registration approaches [7][15][16]. Although it is possible for tensor-product  $B$ -splines to describe sharp features when the corresponding knots collapse, such features can not lie in arbitrary direction due to the regular domain of  $B$ -splines.

In this paper, we propose a novel non-rigid registration algorithm in which the recovered deformation field is represented by triangular  $B$ -splines. We first build the domain triangulation and adjust corresponding knots to the boundaries of pre-segmented rigid structures. As a result, the  $C^0$  continuity is guaranteed at the desired places in the displacement field. The landmarks, selected at the vicinities of rigid objects, are brought into correspondence between source and target images as point-based constraints. The optimal transformation is then estimated by minimizing a composite energy function, which measures image discrepancy, deformation distortion, and desired local rigidities. Empowered by the numerous advantages of triangular  $B$ -splines, such as flexible domain, local control, space-varying smoothness modeling, etc., our registration approach makes the following contributions: The local linear motion in the global non-rigid transformation, caused by rigid structures, can be accurately recovered using relatively fewer degrees of freedom (DOFs), as long as the feature lines are properly aligned in the domain triangulation. With  $C^0$  continuity modeled at the interface between rigid and non-

rigid objects, the deformable region nearby can move more freely and tend to improve the registration quality considerably.

## 2 Theory and Construction of Triangular $B$ -splines

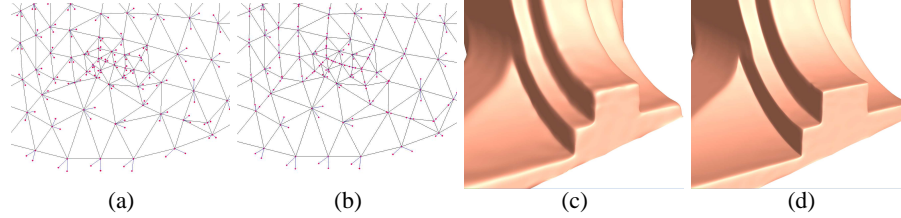


**Fig. 1.** Modeling sharp features using triangular  $B$ -spline with degenerate knots. (a) The domain triangulation and regular knot configurations (no three knots in a domain triangle are collinear). (b) Place the sub-knots along the user-specified edges of domain triangulation. (c) A cubic spline surface reconstructed using the knot configurations in (a). The spline is  $C^2$  continuous everywhere. (d) A cubic spline surface reconstructed using the knot configurations in (b). The spline is  $C^2$  continuous on smooth regions and  $C^0$  on sharp features. appropriately, we can model

Triangular  $B$ -splines, introduced by Dahmen, Micchelli and Seidel[17], have numerous desirable properties for geometric design, such as their automatic smoothness, the ability to define a surface over arbitrary triangulation, and modeling sharp features between any desired adjacent primary knots [18]. Pfeifle and Seidel[19] presented an efficient algorithm to evaluate quadratic triangular  $B$ -splines and Franssen *et al.*[20] extended it to triangular  $B$ -splines of arbitrary degree.

The construction of triangular  $B$ -spline is as follows: let points  $\mathbf{t}_i \in \mathbb{R}^2$ ,  $i \in \mathbb{N}$ , be given and define a triangulation

$$T = \{\Delta(I) = [\mathbf{t}_{i_0}, \mathbf{t}_{i_1}, \mathbf{t}_{i_2}] : I = (i_0, i_1, i_2) \in \mathcal{I} \subset \mathbb{N}^2\}$$

of a bounded region  $D \subseteq \mathbb{R}^2$ . Next, with every vertex  $\mathbf{t}_i$  of  $T$  we associate a cloud of knots  $\mathbf{t}_{i,0}, \dots, \mathbf{t}_{i,n}$  such that  $\mathbf{t}_{i,0} = \mathbf{t}_i$ . The knots  $\mathbf{t}_{i,0} | i \in \mathbb{N}$  are called primary knots, and  $\mathbf{t}_{i,j} | i \in \mathbb{N}, j \geq 1$  are called sub-knots. For every triangle  $I = [\mathbf{t}_{i_0}, \mathbf{t}_{i_1}, \mathbf{t}_{i_2}] \in T$ ,

1. all the triangles  $[\mathbf{t}_{i_0,\beta_0}, \mathbf{t}_{i_1,\beta_1}, \mathbf{t}_{i_2,\beta_2}]$  with  $\beta = (\beta_0, \beta_1, \beta_2)$  and  $|\beta| = \sum_{i=0}^2 \beta_i \leq n$  are non-degenerate.
2. the set

$$\text{interior}(\cap_{|\beta| \leq n} X_\beta^I) \neq \emptyset, X_\beta^I = [\mathbf{t}_{i_0,\beta_0}, \mathbf{t}_{i_1,\beta_1}, \mathbf{t}_{i_2,\beta_2}]. \quad (1)$$

3. If  $I$  has a boundary edge, say,  $(\mathbf{t}_{i_0}, \mathbf{t}_{i_1})$ , then the entire area  $[\mathbf{t}_{i_0,0}, \dots, \mathbf{t}_{i_0,n}, \mathbf{t}_{i_1,0}, \dots, \mathbf{t}_{i_1,n}]$  must lie outside of the domain.

Then the triangular  $B$ -spline basis function  $N_\beta^I$ ,  $|\beta| = n$ , is defined by means of simplex splines  $M(\mathbf{u}|V_\beta^I)$  (for details about simplex splines, please refer to [21]) as

$$N(\mathbf{u}|V_\beta^I) = |d_\beta^I| M(\mathbf{u}|V_\beta^I),$$

where  $V_\beta^I = \{\mathbf{t}_{i_0,0}, \dots, \mathbf{t}_{i_0,\beta_0}, \dots, \mathbf{t}_{i_2,0}, \dots, \mathbf{t}_{i_2,\beta_2}\}$  and

$$d_\beta^I = \det(X_\beta^I) = \det \begin{pmatrix} 1 & 1 & 1 \\ \mathbf{t}_{i_0,\beta_0} & \mathbf{t}_{i_1,\beta_1} & \mathbf{t}_{i_2,\beta_2} \end{pmatrix}.$$

Assuming (1), these  $B$ -spline basis functions can be shown to be all non-negative and to form a partition of unity. Then, the triangular  $B$ -spline is defined as

$$\mathbf{F}(\mathbf{u}) = \sum_{I \in \mathcal{I}} \sum_{|\beta|=n} \mathbf{c}_{I,\beta} N(\mathbf{u}|V_\beta^I), \quad (2)$$

where  $\mathbf{c}_{I,\beta}$  is the control point. This spline is globally  $C^{n-1}$  continuous if all the sets  $X_\beta^I, |\beta| \leq n$  are affinely independent.

One favorable advantage given by triangular  $B$ -splines is that by adjusting sub-knots to the feature lines explicitly, we can model local sharp features (*i.e.*,  $C^0$  continuity) in the approximated space, while keeping the  $C^{n-1}$  smoothness over the other regions. This feature is demonstrated in a surface reconstruction example shown in Fig.1.

### 3 Method

Given source image  $I_s$ , and target image,  $I_t$ , defined on the domain  $\Omega \subset \mathbb{R}^2$ , the problem of registration is to find an optimal geometrical transformation  $\mathbf{T} : \Omega \rightarrow \mathbb{R}^2$  such that the pixels in both images are matched properly.

#### 3.1 Transformation Model

To reduce the global geometric differences between  $I_s$  and  $I_t$ , an initial alignment is achieved using conventional rigid registration algorithm. This obtained transformation will be used as the initial estimation for the following registration.

The concept of free-form deformation (FFD) is to deform an object by manipulation underlying control points. In our work, the FFD is decomposed as an identity transformation plus a displacement field, which is represented by triangular  $B$ -splines as:

$$\mathbf{T}(\mathbf{x}) = \mathbf{x} + \mathbf{u} = \mathbf{x} + \sum_{i=1..m} \phi_i B_i(\mathbf{x}), \quad (3)$$

where  $\phi_i$  is the control point and  $B_i$  is the associated basis function.

Unlike tensor-product  $B$ -spline based FFD[15], whose domain is a rectangular lattice, our triangular  $B$ -spline based FFD has its domain built upon a tessellation of either triangles for 2D or tetrahedra for 3D. It is not difficult to triangulate the reference image domain  $\Omega$  using established techniques. In order to model the sharp features (see Fig.3(c)) at the boundaries of pre-identified rigid bodies, we have to keep them in the triangulated tessellation. Such constraints can be satisfied using the triangulation algorithm proposed by Shewchuk[22]. According to the definition of triangular  $B$ -splines,

the free-form deformation field has  $C^{n-1}$  continuity everywhere if there is no degeneracy for any triple of knots in the same triangle. However, we purposely collapse adjacent sub-knots to pre-identified feature lines in order to model desired  $C^0$  continuity.

Due to the flexibility of the domain triangulation, it is also possible for users to overlay the registration domain exactly upon the region of interest (ROI), rather than covering the entire reference image. Thus, the computational effort will be saved considerably, especially when the ROI can be successfully extracted.

### 3.2 Point-based Constraints

Point-based constraints are incorporated in our framework for better registration. The points on the boundary contours of rigid structure with high curvature are good candidates for landmarks (see Fig.3(d)). Assuming strict rigidity of bony structures, only two pairs of landmarks are required to fully recover local linear transformation (*i.e.*, translation and rotation), if there is no rotoinversion. In practice, we often introduce more constraints to ensure the stability of the registration.

Let  $\mathcal{P} = \{\mathbf{p}_1, \dots, \mathbf{p}_n\}$  be the set of landmarks chosen on the reference domain ( $I_t$  in our implementation). Their correspondences in  $I_s$  are  $\mathcal{Q} = \{\mathbf{q}_1, \dots, \mathbf{q}_n\}$  such that:

$$\mathbf{T}(\mathbf{p}_j; \Phi) = \mathbf{q}_j \quad \text{for } j = 1 \dots n, \quad (4)$$

where  $\Phi$  denotes the set of the control points of triangular  $B$ -splines. The above equations are treated as hard constraints and have to be strictly satisfied in the following optimization process. In most cases, the linear system of (4) is under-determined. But it is possible to become over-constrained when excessive landmarks are selected on a single spline patch. Two approaches can be used to solve such problem. One is to subdivide the triangular mesh, where there are overly-condensed landmarks, and re-initialize the domain triangulation. The drawback of it is that the problem dimension is increased accordingly. The other approach aims to find a compromised solution for (4), which will be discussed later.

### 3.3 Cost Function

In this paper, we register  $I_s$  to  $I_t$  using a variational approach, in which a metric measuring image similarity and constraints of global smoothness and local rigidity are combined into an overall cost function  $E_{total}$  that is defined as:

$$E_{total} = \alpha E_I + \beta E_R + \gamma E_S, \quad (5)$$

where  $\alpha$ ,  $\beta$ , and  $\gamma$  control the relative influence among three energy terms. In (5),  $E_I$  is the driving force behind the registration process and aims to maximize the image similarity, whereas  $E_R$  is a constraint term to ensure local rigidity and  $E_S$  tries to regularize the transformation as smooth as possible.

A number of approaches have been proposed in literature to calculate either similarity or dissimilarity between images. Mutual information[23][24] and correlation ratio[25] are the methods to measure image similarities, while the sum-of-squared-difference (SSD) measures the dissimilarities. In our current work, we simply use SSD

metric to test the feasibility of our registration algorithm. The differences between  $I_s$  and  $I_t$ , represented by  $E_I$ , is evaluated by:

$$E_I = \frac{1}{2} \int_{\Omega} \|I_s(\mathbf{T}(\mathbf{x}; \Phi)) - I_t(\mathbf{x})\|^2 d\mathbf{x}. \quad (6)$$

In the theory of continuum physics, the non-rigid transformation is often measured by *Green-St. Venant* strain tensor  $\mathbf{E}$ . Then a necessary and sufficient condition to obtain a local rigid transformation can be re-formulated as  $\mathbf{E} = \nabla \mathbf{u} + \nabla \mathbf{u}^T + \nabla \mathbf{u}^T \nabla \mathbf{u} = 0$ , which enforces the strain tensor  $\mathbf{E}$  to be zero over rigid structures. This is identical to that proposed in [13], where the Jacobian matrices are considered instead. We enforce the rigidity constraint by defining a penalty term as the integral of the *Frobenius* norm of  $\mathbf{E}$ . Since different structures in the image exhibit different deformation properties, and do not need to deform similarly, we introduce a characteristic function  $w(\mathbf{x})$  to separate the rigid objects from deformable regions. The value of  $w(\mathbf{x})$  is 1 on rigid structures and 0 elsewhere. The penalty term for local rigidity is given by:

$$E_R = \frac{1}{2} \int_{\Omega} w(\mathbf{x}) \|\nabla \mathbf{u} + \nabla \mathbf{u}^T + \nabla \mathbf{u}^T \nabla \mathbf{u}\|_F^2 d\mathbf{x}, \quad (7)$$

where  $\|\cdot\|_F$  denotes the *Frobenius* norm.

A regularization term  $E_S$ , measuring the bending energy of a thin plate metal subject to external forces[7][15], is also incorporated to discourage improbable or impossible transformations. It depends on the 2nd derivatives of the deformation and is written as:

$$E_S = \frac{1}{2} \int_{\Omega} (1 - w(\mathbf{x})) \left[ \left\| \frac{\partial^2 \mathbf{u}}{\partial x^2} \right\|^2 + \left\| \frac{\partial^2 \mathbf{u}}{\partial y^2} \right\|^2 + \left\| \frac{\partial^2 \mathbf{u}}{\partial z^2} \right\|^2 + 2 \left( \left\| \frac{\partial^2 \mathbf{u}}{\partial x \partial y} \right\|^2 + \left\| \frac{\partial^2 \mathbf{u}}{\partial y \partial z} \right\|^2 + \left\| \frac{\partial^2 \mathbf{u}}{\partial x \partial z} \right\|^2 \right) \right] d\mathbf{x}, \quad (8)$$

where the function  $w(\mathbf{x})$  makes the regularization term valid only over non-rigid regions.

### 3.4 Optimization

The optimization problem is stated to find an ideal  $\Phi$  such that the overall energy (5) is minimized with the constraints in (4) satisfied. There are various algorithms available to accomplish such constrained nonlinear programming task. In particular, we convert the constrained optimization problem to an unconstrained one, rather than applying established methods directly. Then a simplex line search approach described in [26] is performed to update the parameters iteratively along the steepest descent of gradient until the cost function can not be decreased any further.

Putting (3) and (4) together, we discretize the point-based constraints and write them in a matrix format:

$$\mathbf{P} + \mathbf{C}\Phi = \mathbf{Q}, \quad (9)$$

where  $\mathbf{P}$  and  $\mathbf{Q}$  are the vectors collecting the landmark positions in  $I_t$  and  $I_s$  respectively, the vector  $\Phi$  consists of the control points of triangular  $B$ -splines, and the triangular  $B$ -spline basis functions constitute the matrix  $\mathbf{C}$  which is extremely sparse and rank-deficient.

By solving the original optimization problem in the Null-Space of  $\mathbf{C}$ , we can successfully remove the point-based constraints. Then, the new parameter vector  $\Psi$  in Null-Space is related to the old one  $\Phi$  by the equation:

$$\Phi = \mathbf{N}\Psi + \Phi_0, \quad (10)$$

in which  $\mathbf{C}\mathbf{N} = 0$  and  $\mathbf{C}\Phi_0 = \mathbf{Q} - \mathbf{P}$ . We use Gaussian-Jordan-Elimination-like approach proposed in [27] to construct  $\mathbf{N}$ , and solve for  $\Phi_0$  by either singular value decomposition (SVD) or QR decomposition, both of which are computationally viable here, since most columns in  $\mathbf{C}$  are zero.

Instead of estimating the gradient of  $E_{total}$  using finite-difference approximation, we analytically calculate the derivative with respect to  $\Psi$  and obtain:

$$\frac{\partial E_{total}}{\partial \Psi} = \mathbf{N}^T \left( \alpha \frac{\partial E_I}{\partial \Phi} + \beta \frac{\partial E_R}{\partial \Phi} + \gamma \frac{\partial E_S}{\partial \Phi} \right), \quad (11)$$

where

$$\frac{E_I}{\partial \phi_i} = \int_{\Omega} (I_s(\mathbf{T}(\mathbf{x})) - I_t(\mathbf{x})) \nabla I_s |_{\mathbf{T}(\mathbf{x})} B_i(\mathbf{x}) d\mathbf{x}.$$

Let  $\phi_{ij}$  denotes the  $(3i + j)$ -th component of  $\Phi$  and  $B_{i,j}$  be the derivative of the basis function in  $j$  direction, where  $j = 1, 2, 3$  for  $x, y$  and  $z$  coordinates, respectively. The derivative of the local rigidity penalty term is:

$$\begin{aligned} \frac{E_R}{\partial \phi_{ij}} &= \int_{\Omega} w(\mathbf{x}) \sum_{s,t=1,2,3} \mathbf{M}_{st} \frac{\partial \mathbf{M}_{st}}{\partial \phi_{ij}} d\mathbf{x} \\ \mathbf{M}_{st} &= \sum_{\substack{k=1\dots m \\ r=1,2,3}} \phi_{kt} B_{k,s} + \phi_{ks} B_{k,t} + \phi_{ks} \phi_{kt} B_{k,r}^2 \\ \frac{\partial \mathbf{M}_{st}}{\partial \phi_{ij}} &= \sum_{r=1,2,3} \delta_{jt} (B_{i,s} + \phi_{is} B_{i,r}^2) + \delta_{js} (B_{i,t} + \phi_{it} B_{i,r}^2) \end{aligned}$$

in which  $\delta_{ij}$  is *Dirac* function which equals to 1 if and only if  $i = j$ . Likewise, the derivative of the regularization term is given by:

$$\frac{E_S}{\partial \phi_{ij}} = \int_{\Omega} (1 - w(\mathbf{x})) \left( \sum_{s,k=1,2,3} \phi_{kj} B_{k,s} B_{i,s} + \sum_{s,t,k=1,2,3} \phi_{k,j} B_{k,st} B_{i,st} \right) d\mathbf{x},$$

where  $B_{i,st}$  stands for the second derivative of basis functions. For details on efficient evaluation of triangular  $B$ -spline basis functions and their derivatives, please refer to [19][20][28].

Note that the integration operation in (5) is performed only on the pixels of ROI. Therefore, we could significantly speedup the registration procedure if all the basis functions and their derivatives over the interested region are pre-computed.

## 4 Experimental Results

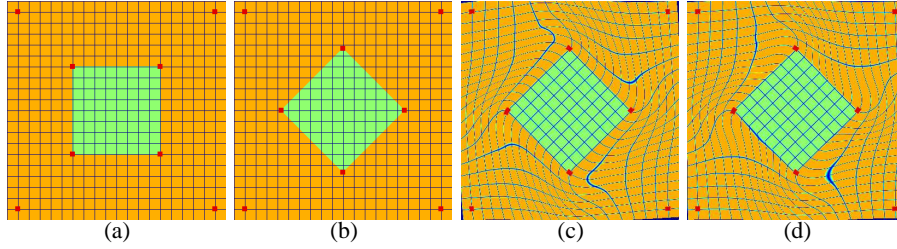


**Fig. 2.** The first experiment: (a) Source image. (b) Target image. (c) Registration result when sharp features are NOT modeled. The minimized energy terms are  $E_S = 97.6$ ,  $E_R = 39.9$ . (d) Registration result when sharp features are modeled, the minimized energy terms are  $E_S = 71.8$ ,  $E_R = 30.8$ .

In order to evaluate the feasibility and applicability of the proposed algorithm, we test it on both synthetic and real data. Cubic triangular  $B$ -splines are chosen in the experiments to compare with the frequently used cubic tensor-product  $B$ -splines.

The first example demonstrated in Fig.2 doesn't consider matching image intensities (*i.e.*,  $\alpha = 0$  in (5)), but tries to align corresponding points instead. A green square is included in the source image to represent a rigid object, and its counterpart is included in the target image with a rotation of  $45^\circ$ . 8 pairs of landmarks are selected at the corners of both the image and the rigid square, and applied as the point-based constraints in the registration. The target image is chosen as the reference domain, which is triangulated into 32 patches, and the cubic triangular  $B$ -splines built on it have 361 control points. After applying our algorithm without and with sharp feature modeling respectively, the achieved registration results are plotted in Fig.2(c) and Fig.2(d). It is noticeable that the background and the square are more smoothly connected in Fig.2(c) than in Fig.2(d), because they are treated as a single elastic object in the former one, but considered as separate parts in the latter one. It is more physically appropriate to model  $C^0$  continuity between the background and the square, when we simulate the interaction between them. Therefore, the method with sharp feature modeling can achieve better registration result (the minimized energy terms are  $E_S = 71.8$ ,  $E_R = 30.8$ ) than the other one ( $E_S = 97.6$ ,  $E_R = 39.9$ ), when the same parameter setting ( $\beta = \gamma = 1$ ) is used.

For the second example, both images (see Fig.3(a)(e)) include three geometric objects to represent rigid structures, whose positions are quite different in the source and the target images. The reference domain (shown in Fig.3(b)) has 130 triangles and the triangular  $B$ -splines thus have 631 control points. 13 pairs of landmarks are picked up to ensure correct alignment between rigid structures (see Fig.3(f)). The registration result and the recovered deformation field are shown in Fig.3(g) and Fig.3(h). An alternative approach using tensor-product  $B$ -splines is also applied for the comparison purpose. Its domain is defined on a  $25 \times 25$  to match the number of triangular  $B$ -spline control points. The comparison between the results from both approaches (shown in Fig.3(c))

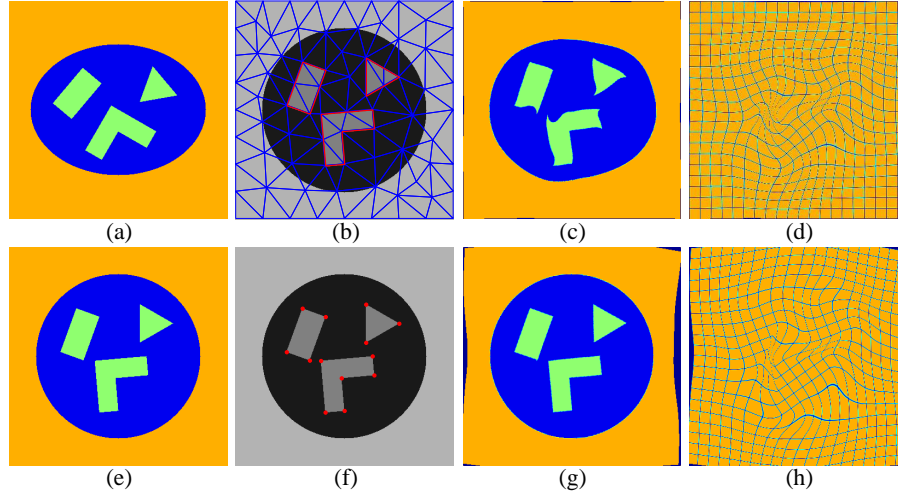


**Fig. 3.** The second experiment: (a) Source image. (e) Target image. (b) The domain triangulation with feature lines highlighted in red. (f) 13 landmarks are highlighted in red. (c) Registration result obtained from tensor-product  $B$ -spline based method. (g) Registration result obtained from triangular  $B$ -spline based method. (d) Deformation recovered using tensor-product  $B$ -spline based method. (h) Deformation recovered using triangular  $B$ -spline based method.

and Fig.3(g)) indicates that the tensor-product based method fails to align the images at a desired resolution, when there exist large deformations near rigid structures. In sharp contrast, triangular  $B$ -spline is built on a flexible domain, so that its modeling power can be ideally concentrated on the interested region for better registration. Furthermore, its power of modeling sharp features helps to improve the registration quality far more better.

Two MRI images of human spines (see Fig.4(a)(b)) are used in the third experiment. The spinal bones are first segmented from the target image, then the characteristic function  $w$  is set accordingly to decide where the rigidity constraints should be applied. The source image is registered to the target image as shown in Fig.4, in which all of the rigid structures are successfully matched.

Our algorithm is implemented using MS VC++, and all experiments are conducted on a platform with 2.8GHz Pentium IV CPU and 1G RAM. Both synthetic images have the size of  $400 \times 400$ , and the size of the MRI images used for the third experiment is  $512 \times 512$ . The running time for the three experiments are about 1 minute, 6 minutes, and 12 minutes respectively.

## 5 Discussion and Conclusion

This paper presents a nonrigid registration technique in which the transformation between corresponding images are represented by triangular  $B$ -splines. By preserving feature lines in the domain triangulation and adjusting knots accordingly, the proposed

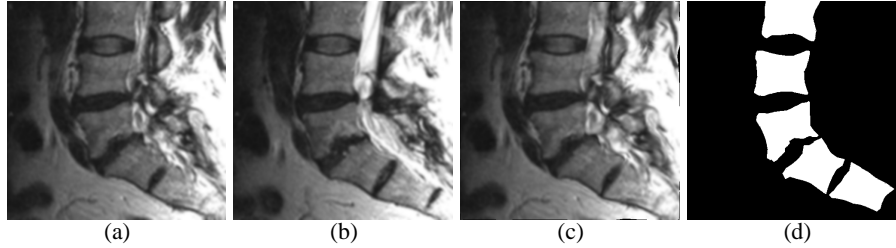


**Fig. 4.** The third experiment: (a) Source image. (b) Target image. (c) Registration result. (d) Rigid structures segmented from the target image.

method successfully recovers local rigid motions and accurately simulates  $C^0$  continuities at desired regions, using relatively fewer degrees of freedom and lower degree polynomials. The actual registration is done through the use of a variational framework, in which a constrained optimization problem is solved to reduce the differences between images and enforce both local rigidity and global smoothness at the same time. The method has been tested on both synthetic examples and real data for its efficacy.

Although tensor-product  $B$ -spline based approaches are still dominating in the field of non-rigid registration, their applicability is somehow limited due to the structure of their regular domain. On the contrary, our registration method can correctly delineate the boundaries of rigid bodies in its domain triangulation at a much coarser level, and thus model the local rigid motions more accurately. Furthermore, with the degenerate knots on the boundaries of rigid structures,  $C^0$  continuity is automatically guaranteed in the described displacement field, and can be naturally coupled with the optimization process. This advantage enables us to precisely simulate the behavior of rigid objects inside elastic tissues. From the registration point of view, the deformable regions around the rigid structures may become less constrained by the regularization term and contribute extra flexibility to the minimization of the cost function (5). As a result, the registration quality can be considerably improved. An alternative way to model  $C^0$  continuities could be to separate rigid and non-rigid regions into different domain pieces. However, extra efforts must be spent to keep the overall transformation consistent across different pieces in a different hierarchy, and in general, the variational approaches over irregular domains in a hierarchical fashion have not been fully explored. In this paper, only rigid structures with simple geometric shapes are considered in our experiments for the feasibility test. To accommodate more complicated structures, we can subdivide the domain mesh adaptively along their boundaries until the desired accuracy is achieved. The landmarks applied in our registration are interactively selected by users based on their knowledge and subjectivity. Naturally, the registration result is affected by the quality of landmark selection.

There are a few possible extensions to our current work. Although only the registration of two dimensional images is considered in this paper, it is much more natural to extend it to the area of volumetric data registration, and trivariant tetrahedral  $B$ -splines shall be exploited. Alternative metrics measuring image similarities, such as mutual information and normalized correlation, can be incorporated into our variational frame-

work to deal with multi-modality registration. One limitation of our current approach is the necessity for image segmentation and landmark selection prior to our registration procedure. It would be ideal to have an automated method to select landmarks, segment images into different pieces, and accurately match corresponding rigid structures in order to streamline the task of medical image processing.

## Acknowledgements

This research was partially supported by the NSF grant ACI-0328930, the ITR grant IIS-0326388, and the Alfred P. Sloan Fellowship.

## References

1. Brown, L.G.: A survey of image registration techniques. *ACM Comput. Surv.* **24** (1992) 325–376
2. Maintz, J., Viergever, M.: A survey of medical image registration. *Medical Image Analysis* **2** (1998) 1–36
3. Zitová, B., Flusser, J.: Image registration methods: a survey. *Image Vision Comput.* **21** (2003) 977–1000
4. Peters, T., Davey, B., Munger, P., Comeau, R., Evans, A., Olivier, A.: Three-dimensional multimodal image-guidance for neurosurgery. *IEEE Transactions on medical imaging* **15** (1996) 121–128
5. Potamianos, P., Davies, B., Hibberd, R.D.: Intraoperative registration for percutaneous surgery. In: *First International Symposium on Medical Robotics and Computer Assisted Surgery*. Volume 1. (1995) 98–105
6. Cachier, P., Mangin, J.F., Pennec, X., Rivière, D., Papadopoulos-Orfanos, D., Régis, J., Ayache, N.: Multisubject non-rigid registration of brain mri using intensity and geometric features. In: *MICCAI*. (2001) 734–742
7. Rueckert, D., Sonoda, L., Hayes, C., Hill, D.L., Leach, M.O., Hawkes, D.J.: Non-rigid registration using free-form deformations: Application to breast mr images. *IEEE Trans. Med. Imaging* **18** (1999) 712–721
8. Edwards, P.J., Hill, D.L.G., Little, J.A., Sahni, V.A.: Medical image registration incorporating deformations. In: *BMVC*. (1995) 691–699
9. Little, J.A., Hill, D.L.G., Hawkes, D.J.: Deformations incorporating rigid structures. *Computer Vision And Image Understanding* **66** (1997) 223–232
10. Rohr, K., Fornefett, M., Stiehl, H.S.: Spline-based elastic image registration: Integration of landmark errors and orientation attributes. *Computer Vision And Image Understanding* **90** (2003) 153–168
11. Duay, V., D’Haese, P.F., Li, R., Dawant, B.M.: Non-rigid registration algorithm with spatially varying stiffness properties. In: *ISBI*. (2004) 408–411
12. Tanner, C., Schnabel, J.A., Chung, D., Clarkson, M.J., Rueckert, D., Hill, D.L.G., Hawkes, D.J.: Volume and shape preservation of enhancing lesions when applying non-rigid registration to a time series of contrast enhancing mr breast images. In: *MICCAI*. (2000) 327–337
13. Loeckx, D., Maes, F., Vandermeulen, D., Suetens, P.: Nonrigid image registration using free-form deformations with a local rigidity constraint. In: *MICCAI* (1). (2004) 639–646
14. Meyer, C.R., Boes, J.L., Kim, B., Bland, P.H., Zasadny, K.R., Kison, P.V., Koral, K., Frey, K.A., Wahl, R.L.: Demonstration of accuracy and clinical versatility of mutual information for automatic multimodality image fusion using affine and thin-plate spline warped geometric deformations. *Med. Image Anal.* **1** (1996/7) 195–206

15. Rohlfing, T., Jr., C.R.M., Bluemke, D.A., Jacobs, M.A.: An alternating-constraints algorithm for volume-preserving non-rigid registration of contrast-enhanced mr breast images. In: WBIR. (2003) 291–300
16. Vemuri, B.C., Huang, S., Sahni, S., Leonard, C.M., Mohr, C., Gilmore, R., Fitzsimmons, J.: An efficient motion estimator with application to medical image registration. *Medical Image Analysis* **2** (1998) 79–98
17. Dahmen, W., Micchelli, C.A., Seidel, H.P.: Blossoming begets b-spline built better by b-patches. *Mathematics of Computation* **59** (1992) 97–115
18. Fong, P., Seidel, H.P.: An implementation of triangular b-spline surfaces over arbitrary triangulations. *Computer Aided Geometric Design* **10** (1993) 267–275
19. Pfeifle, R., Seidel, H.P.: Faster evaluation of quadratic bivariate b-spline surfaces. In: *Proceedings of Graphics Interface'94*. (1994) 182–189
20. Franssen, M., Veltkamp, R.C., Wesselink, W.: Efficient evaluation of triangular b-spline surfaces. *Computer Aided Geometric Design* **17** (2000) 863–877
21. Micchelli, C.A.: On a numerically efficient method for computing multivariate b-splines. *Multivariate approximation theory* (**51**) 211–248
22. Shewchuk, J.R.: Automated three-dimensional registration of magnetic resonance and positron emission tomography brain images by multiresolution optimization of voxel similarity measures. *Med. Phys.* **24** (1997) 25–35
23. Collignon, A.: Multi-modality medical image registration by maximization of mutual information. PhD thesis, Catholic University of Leuven, Leuven, Belgium (1998)
24. Viola, P.A.: Alignment by maximization of mutual information. PhD thesis, Massachusetts Institute of Technology, Boston, MA, USA (1995)
25. Roche, A., Malandain, G., Pennec, X., Ayache, N.: The correlation ratio as a new similarity measure for multimodal image registration. In: *MICCAI*. (1998) 1115–1124
26. Press, W.H., Teukolsky, S.A., Vetterling, W.T., Flannery, B.P.: *Numerical Recipes in C: The Art of Scientific Computing*. Cambridge University Press (1992)
27. Gill, P., Murray, W., Wright, M.: *Practical Optimization*. Academic Press (1981)
28. He, Y., Qin, H.: Surface reconstruction with triangular b-splines. In: *GMP*. (2004) 279–290